



Geophysical Research Letters

RESEARCH LETTER

10.1029/2020GL089583

Key Points:

- We discovered reidite, a high-pressure polymorph of $ZrSiO_4$, in the regolith breccia of lunar meteorite Sayh al Uhaymir 169
- The reidite could have formed under localized transient pressure spikes during initial stage of asteroid impact into porous lunar regolith
- High postshock temperature of porous lunar regolith likely inhibits the widespread preservation of high-pressure polymorphs in lunar samples

Supporting Information:

- Supporting Information S1

Correspondence to:

Y. Lin,
linyt@mail.igcas.ac.cn

Citation:

Xing, W., Lin, Y., Zhang, C., Zhang, M., Hu, S., Hofmann, B. A., et al. (2020). Discovery of reidite in the lunar meteorite Sayh al Uhaymir 169. *Geophysical Research Letters*, 47, e2020GL089583. <https://doi.org/10.1029/2020GL089583>

Received 30 JUN 2020

Accepted 14 OCT 2020

Accepted article online 20 OCT 2020

Discovery of Reidite in the Lunar Meteorite Sayh al Uhaymir 169

HPSTAR
1051-2020

Weifan Xing^{1,2} , Yangting Lin^{2,3} , Chi Zhang² , Mingming Zhang² , Sen Hu² , Beda A. Hofmann^{4,5} , Toshimori Sekine⁶ , Long Xiao¹ , and Lixin Gu²

¹School of Earth Sciences, China University of Geosciences, Wuhan, China, ²Key Laboratory of Earth and Planetary Physics, Institute of Geology and Geophysics, Chinese Academy of Sciences, Beijing, China, ³College of Earth and Planetary Sciences, University of Chinese Academy of Sciences, Beijing, China, ⁴Natural History Museum Bern, Bern, Switzerland, ⁵Institute of Geological Sciences, University of Bern, Bern, Switzerland, ⁶Center for High Pressure Science & Technology Advanced Research, Shanghai, China

Abstract An exceedingly small number of high-pressure polymorphs have been discovered in lunar samples. This situation does not seem to reconcile with the prolonged, intense bombardment of the lunar surface, which should produce suitable conditions for the formation of such polymorphs. Here we report the discovery of reidite, a high-pressure polymorph of $ZrSiO_4$ with scheelite structure in lunar meteorite Sayh al Uhaymir (SaU) 169. The reidite occurs mainly as lamellae hosted within zircon, likely corresponding to a deviatoric-dominated transformation. The presence of reidite in the regolith portion of SaU 169 indicates a narrow temperature and pressure path constrained by the phase stability under low pressure and suggests heterogeneous shock features in the porous lunar regolith where the ambient temperature increases much higher than that in compact rocks. The inventory of high-pressure polymorphs might be restricted by such unusual cooling processes lunar samples experienced.

Plain Language Summary The most striking phenomenon on the Moon's surface is the densely distributed impact craters. Asteroid impacts generate high pressure and temperature conditions, resulting in the formation of high-pressure minerals. However, only few high-pressure minerals have been discovered in very few lunar samples so far. In this study, we first discovered reidite, a high-pressure polymorph of $ZrSiO_4$, in the regolith portion of lunar meteorite Sayh al Uhaymir (SaU) 169. Previous research produced reidite by applying shock pressure of >30 GPa on zircon and found that it back-transformed to zircon quickly at temperature of >1473 K under ambient pressure. Impact into porous lunar regolith will lead to a huge increase in ambient temperature. For a postshock temperature of <1473 K, the estimated average peak pressure should not have exceeded ~ 10 GPa. Therefore, we suggest that reidite formed in localized high-pressure regions (>30 GPa) induced by an impact with an average peak pressure <10 GPa. In addition, shock-induced high ambient temperature conditions in porous lunar regolith are not favorable for the preservation of most high-pressure minerals, therefore might restrict the observation of high-pressure minerals in lunar samples which were mostly derived from the porous regolith layer.

1. Introduction

Asteroid impacts are the most common and important processes modifying the surface and near-surface of the Moon (e.g., Hiesinger & Head, 2006; Stöffler et al., 2006). Extremely high pressure, temperature, and strain rate associated with impacts can cause shock metamorphism in target materials (Bischoff & Stöffler, 1992; French, 1998; Langenhorst & Deutsch, 2012). However, high-pressure phase transformation, one of the most diagnostic features of impact events, seems to be rare in lunar samples: only two high-pressure polymorphs of olivine (ringwoodite and wadsleyite) (Barrat et al., 2005; Zhang et al., 2010) and three high-pressure minerals of silica (coesite, stishovite, and seifertite) (Miyahara et al., 2013; Ohtani et al., 2011) have been found in very few lunar samples so far. In contrast, high-pressure polymorphs of almost all constituent minerals (silicates, oxides, and phosphates) have been discovered in the highly shocked ordinary chondrites and Martian meteorites (El Goresy et al., 2013; Tomioka & Miyahara, 2017).

Zircon, the most common mineral for U-Pb chronology, also preserves a variety of shock-induced microstructures (Corfu et al., 2003; Timms et al., 2012, 2017; Wittmann et al., 2006). It is a common accessory

mineral in a very K-, REE-, and P-rich (KREEP-rich) lunar meteorite Sayh al Uhaymir (SaU) 169. The meteorite consists of two lithologies: ~87 vol% is a crystalline fine-grained impact melt breccia, and ~13 vol% is a shock-lithified regolith breccia, both are polymict breccia containing a wide range of fragment types (Gnos et al., 2004). The lunar meteorite SaU 169 experienced a protracted thermal history inferred from multiple isotopic systems (Gnos et al., 2004; Lin et al., 2012; D. Liu et al., 2012). We investigated the shock-induced microstructures of zircon within the regolith breccia of SaU 169 using a field emission scanning electron microscope (FE-SEM), laser Raman spectroscopy, and a synchrotron X-ray diffractometer (XRD) and report the first discovery of reidite, a high-pressure polymorph of $ZrSiO_4$, in a lunar sample.

2. Materials and Methods

Four polished thick sections (labeled as A, C, E, and G; Figure S1 in the supporting information) were made out of a fragment of the regolith portion of SaU 169. All experiments were carried out at the Institute of Geology and Geophysics, Chinese Academy of Sciences (IGGCAS), except for the synchrotron XRD, which was carried out at the Shanghai Synchrotron Radiation Facility (SSRF). A search of reidite-bearing zircons was performed using an FEI Nova NanoSEM 450 FE-SEM equipped with an Oxford X-MAX^N 80 energy dispersive spectrometer (EDS), a Gatan MonCL4 cathodoluminescence (CL) detector, and an Oxford Nordlys Nano electron backscatter diffraction (EBSD) detector. For EBSD measurements, section A was repolished with 0.05 μm colloidal silica to remove the deformation layer of the surface. However, the sections C, E, and G were not reprocessed because of their poor resin conditions. The EBSD analyses were conducted by scanning an electron beam of 10–20 nm over the sample tilted 70° relative to the horizon, with an accelerating voltage of 18 kV and a working distance of 20 mm. The step size for the whole reidite-bearing grain was 0.8 μm , while for the restricted reidite domain region within a grain it was 0.07 μm . EBSD maps and pole figures were generated using the integrated Oxford Instruments AZtecHKL and Channel 5 software to illustrate the phase distributions and crystallographic orientations. The EBSD data were initially noise reduced by infilling isolated nonindexed pixels and removing “wildspikes” with an average orientation based on a five nearest neighbor extrapolation. Laser Raman spectroscopic analysis was conducted with a LabRam HR800 microspectrometer, using a laser beam with a wavelength of 633 nm, a beam size of 1 μm , and a power of 10 mW. A single crystal of silicon (peak at 520.5 cm^{-1}) was used to calibrate the spectrometer. A Zeiss Auriga Compact dual beam focused ion beam (FIB) equipped with an Omniprobe AutoProbe 200 micromanipulator was used to prepare a FIB slice of the reidite-bearing zircon C-13 for synchrotron XRD analysis. After cutting, the ~1.5 μm thick FIB slice was transferred and welded onto a Cu grid by depositing Pt. The slice mounted on the Cu grid was then scanned using X-rays at the BL15U1 beamline, SSRF. The monochromatic beam (~5 μm in diameter) had a wavelength of 0.6199 \AA , and the signal was counted with a charge-coupled device (CCD) detector. The orientation of the detector and its distance to the sample were calibrated with a CeO_2 standard. The two-dimensional diffraction patterns collected on the CCD detector were integrated by using the Fit2D software (Hammersley et al., 1996). The determined space distances and intensities of lunar reidite are listed together with those of terrestrial (Chen et al., 2013) and synthetic reidite (L. Liu, 1979) in Table S1.

3. Results

The studied samples are from the regolith portion of SaU 169, consisting of numerous fractured lithic clasts and mineral fragments welded together by shock-induced glassy matrix (Figure S1). These clastic materials could have derived from different kinds of lunar rock types such as magnesium suite, alkali suite, ferroan anorthosites, and mare basalts, as well as various impact melt breccia (Figure S1). Forty zircons with sizes ranging from ~5 to ~140 μm on four thin sections (A, C, E, and G) of SaU 169 have been investigated, of which four zircons have been found to contain reidite (Figures 1, 2, and S1): Zircon E-8 is a $20 \times 35 \mu\text{m}^2$ anhedral mineral fragment embedded in a small melt vein; zircon C-13 is a $3 \times 6 \mu\text{m}^2$ anhedral grain attached to a partially melted plagioclase grain in a shocked lithic clast composed of plagioclase, pyroxene, and zircon; zircon G-1 is a $5 \times 8 \mu\text{m}^2$ anhedral mineral clast enclosed in an impact melt clast dominated by fine-grained pyroxene and plagioclase, and zircon A-6 is a $20 \times 140 \mu\text{m}^2$ elongated subhedral mineral clast in the matrix.

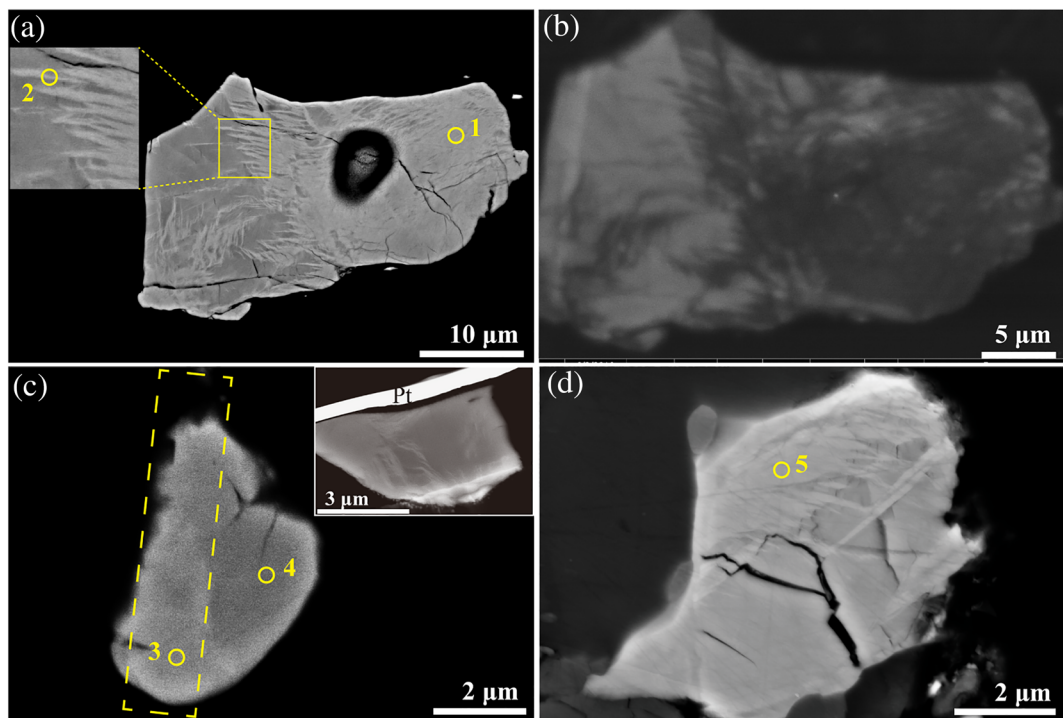


Figure 1. Reidite-bearing zircons. (a) BSE image of zircon E-8. A close-up image of the lamellae is shown in the inset. The pit in the middle of the grain is a NanoSIMS analysis point. (b) CL image of zircon E-8. (c) BSE image of zircon C-13. Yellow box indicates the location of the FIB slice shown in the inset. (d) BSE image of zircon G-1. Abbreviation: Pt = platinum; yellow circles and numbers represent the analysis positions of Raman spectra plotted in Figure 3.

SEM images of zircons E-8, C-13, and G-1 show domains that are brighter in BSE image and darker in CL image than the remaining parts of host grains (Figure 1). The domains contain multiple lamellae with each $<1\text{ }\mu\text{m}$ wide (Figure 1). Raman spectra from these domains show peaks at $\sim 297, 325, 404, 459, 555, 840$, and 884 cm^{-1} that can be attributed to reidite (Erickson et al., 2017; Gucsik et al., 2004; Knittle & Williams, 1993; Wittmann et al., 2006), in addition to peaks at $\sim 202, 352, 435, 973$, and $1,003\text{ cm}^{-1}$ that belong to zircon (Gucsik et al., 2004) (Figure 3). The synchrotron XRD pattern of zircon C-13 shows 16 diffraction lines, of which 4 can be attributed to reidite, 7 to zircon, 2 to both phases, and the remaining 3 to the Cu grid (Figure 4 and Table S1). The diffraction pattern of reidite here is consistent with those of terrestrial reidite (Chen et al., 2013) and synthetic reidite (L. Liu, 1979). A small rhomb-shaped area ($\sim 0.5 \times 2\text{ }\mu\text{m}^2$) within zircon A-6 was indexed as reidite domain via EBSD mapping (Figure 2), similar to the patchy domain form of reidite described by Walton et al. (2019). The orientation relationship between reidite and the host zircon is that $\langle 001 \rangle_{\text{reidite}}$ and $\{110\}_{\text{reidite}}$ are parallel to $\{110\}_{\text{zircon}}$ and $\langle 001 \rangle_{\text{zircon}}$, respectively (Figure 2), as reported in previous work (Erickson et al., 2017; Timms et al., 2017). The remaining parts of the host zircon preserve low-angle misorientation resulting from crystal-plastic deformation and rotation of rigid fractured blocks (Figure 2).

4. Discussions

Though lunar zircon preserved a variety of impact-induced microstructures, such as crystal-plastic deformation, twins, planar fractures, and polycrystalline aggregates (Crow et al., 2017; Grange et al., 2013; Nemchin et al., 2009; Pidgeon et al., 2007, 2011; Timms et al., 2012), reidite has never been discovered in lunar samples, possibly due to a very limited number of zircon grains for comprehensive study. Here we report the first discovery of lunar reidite, the scheelite-structured high-pressure polymorph of ZrSiO_4 , in the regolith portion of SaU 169, providing a new perspective on the impact history of the Moon. The lunar reidite is mainly present as lamellar-textured domain within the host zircons, similar to the form of running products of shock experiments and most natural reidite found in terrestrial impact structures which is usually

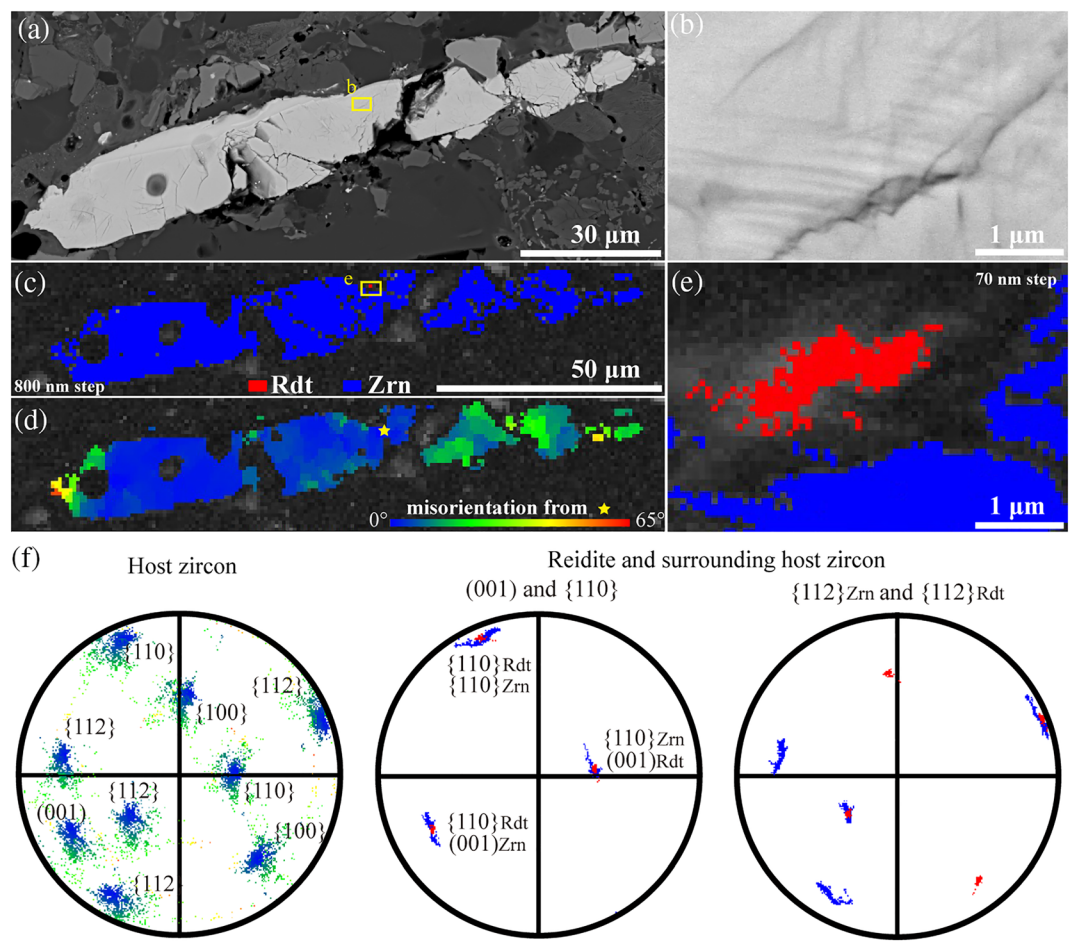


Figure 2. Images and crystallographic data of reidite-bearing zircon A-6. (a) BSE image of zircon A-6. Yellow box shows area in (b). (b) Close-up BSE image of the reidite-bearing domain. (c) Phase map of zircon A-6, with zircon (Zrn) in blue and a small reidite (Rdt) domain in red. Yellow box shows area in (e). (d) Map showing crystallographic orientation of the host zircon, relative to a reference point (yellow star). Width of the view is the same as (c). (e) Close-up phase map of the reidite-bearing domain. (f) Pole figures of the host zircon and reidite (the pole figures are upper hemisphere, equal area projections). Color scheme in (f) correlates to (d) (host zircon) and (c) (reidite and host zircon).

interpreted as a martensitic-like (shear-dominated) transformation (Cavosie et al., 2015; Chen et al., 2013; Erickson et al., 2017; Glass & Liu, 2001; Leroux et al., 1999; Timms et al., 2017). The crystallographic relationship between reidite domain and the host grain in zircon C-13 [$\{001\}_{\text{reidite}}//\{110\}_{\text{zircon}}$ and $\{110\}_{\text{reidite}}//\{001\}_{\text{zircon}}$] indicates that $\langle 110 \rangle_{\text{zircon}}$ was converted to $[001]_{\text{reidite}}$ during phase transition (Erickson et al., 2017; Timms et al., 2017).

The four reidite-bearing zircons occur in different petrographic settings and sizes, that is, as coarse grains (zircon E-8: $20 \times 35 \mu\text{m}^2$; zircon A-6: $20 \times 140 \mu\text{m}^2$) embedded in the matrix, as a fine grain (zircon G-1: $5 \times 8 \mu\text{m}^2$) enclosed in a crystalline melt breccia, and as a fine grain (zircon C-13: $3 \times 6 \mu\text{m}^2$) included in a lithic clast, indicating that the transformations of zircon to reidite might happen separately in individual protoliths. However, since high-pressure minerals have been rarely reported in lunar samples and zircon is an accessory mineral, it is less likely that the four reidite-bearing zircons have different origins and then assembled in a centimeter-scale breccia of SaU 169. Thus, we suggest that the phase transformations of zircon to reidite most likely happened *in situ* within the regolith portion of SaU 169. The finding of reidite in only 4 of 40 grains is also in-line with variable shock effects on the scale of the constituent mineral grains caused by shock compression on highly heterogeneous and/or porous targets like lunar regolith (e.g., Kieffer, 1971; Kieffer et al., 1976).

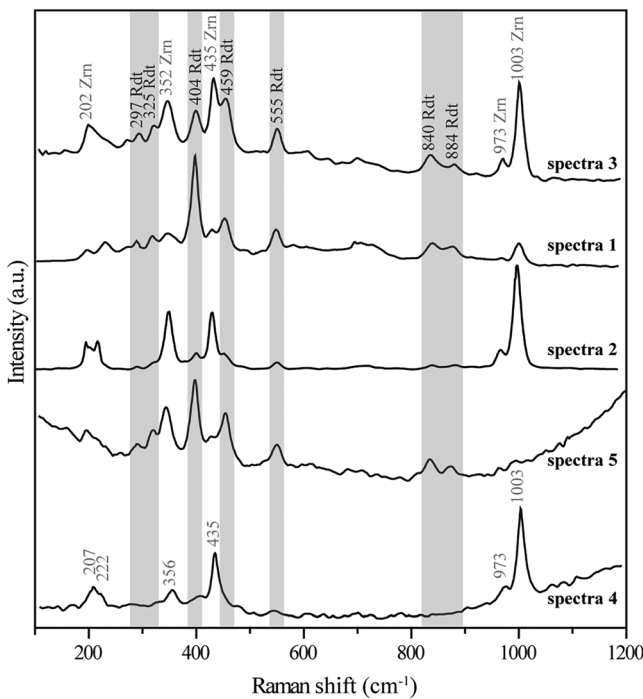


Figure 3. Raman spectra of reidite and zircon domains in zircon E-8 (Spectra 1 and 2), C-13 (Spectra 3 and 4), and G-1 (Spectra 5). Abbreviations are used as previous.

Shock-induced zircon-to-reidite transformation was experimentally achieved at pressure of >30 GPa (Gucsik et al., 2004; Kusaba et al., 1985; Leroux et al., 1999; Timms et al., 2017). Meanwhile, the reversion of reidite to zircon can happen rapidly above 1473 K at ambient pressure (Kusaba et al., 1985). Granular zircon with a systematic orthogonal disorientation relationship ($\sim 90^\circ$ around $<110>$) between neoblasts can be used as an indicator of zircon reversion from reidite (Cavosie et al., 2018; Timms et al., 2017). The preservation of reidite indicates that the post-shock temperature of the host regolith breccia of SaU 169 could not have been above 1473 K. Based on the shock wave equation of state (Hugoniot) data of lunar regolith, an approximate relationship between shock pressure and postshock temperature was obtained, where a temperature of ~ 1473 K corresponds to an average shock pressure of ~ 10 GPa (see Appendix A). The pressure is much lower than the typical pressure for shock-induced transformation of zircon to reidite (>30 GPa). However, the transition could have nevertheless occurred in lunar regolith because the pressure and temperature distribution in highly porous target can be highly spatially and temporally heterogeneous in the initial stages of shock compression (Bland et al., 2014; Davison et al., 2016; Guldemeister et al., 2013; Kowitz et al., 2013). Shock simulations of porous sandstone indicate that localized pressure amplification associated with pore collapse can exceed 4 times the average shock pressure (Kowitz et al., 2013). Numerical modeling of shock compaction on primordial chondritic materials with porous matrix shows that the pressure-temperature varies by >10 GPa and >1000 K over ~ 100 μm with an impact velocity as low as 1.5 km/s (Bland et al., 2014). When pressure is heterogeneous on a millimeter scale, the equilibrium achieves on the microsecond timescale after the initial shock (Baer & Trott, 2002; Davison et al., 2016). Thus, within this time interval, reidite could have formed in localized regions with transient pressure spikes, which corresponds well to the fact that the phase transformation can occur within less than a microsecond in shock recovery experiments (e.g., Gucsik et al., 2004).

Due to the porous nature of lunar regolith (average porosity of the top 2 m is >40 vol%; Heiken et al. 1991), asteroid impacts into it would significantly enhance the ambient temperature as voids collapse (Gibbons et al., 1975; Schaal & Horz, 1980). A postshock temperature of ~ 1473 K can correspond to an average shock pressure of ~ 10 GPa, where the temperature is much higher than that of impacts on compact rocks. For example, the calculated postshock temperature of nonporous chondrite with the composition of Tenham (a Type 6 ordinary chondrite) is only ~ 400 K under a shock pressure of ~ 25 GPa (Xie et al., 2006). Furthermore, average impact velocity on the Moon is >10 km/s that will generate much higher shock pressure and temperature (Ivanov, 2001). However, high ambient temperature condition is not favorable for the preservation of most high-pressure polymorphs of rock-forming minerals (e.g., Dachille et al., 1963; Ito & Navrotsky, 1985). For example, wadsleyite (β - Mg_2SiO_4) back transforms to olivine in seconds at temperatures above 1200 K and ambient pressure (Hu & Sharp, 2017). Up to now, all the samples returned by the Apollo and Luna missions, as well as most lunar meteorites, are derived from the lunar regolith layer (Artemieva & Ivanov, 2004; Lucey et al., 2006; Nishiizumi & Caffee, 2010; Warren, 1994). Among them, regolith breccia consisting of

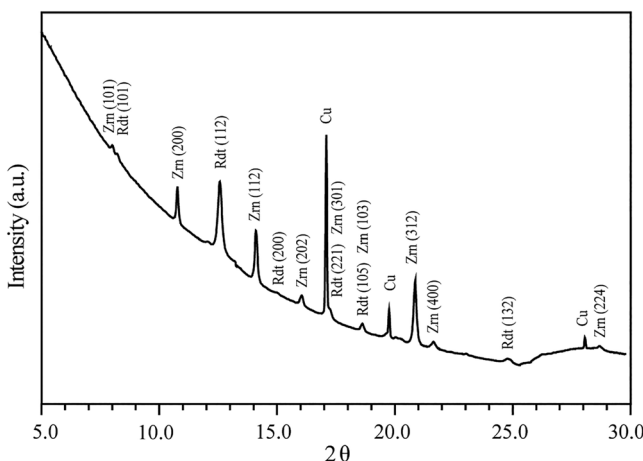


Figure 4. Synchrotron XRD pattern of the FIB slice from zircon C-13. The quantitative data are listed in Table S1. Abbreviations: Cu = copper grid; others are used as previous.

shock-lithified lunar regolith is a major rock type (Wieczorek et al., 2006). As most lunar samples reflect the nature of regolith, shock-induced high-temperature conditions might be a possible reason for the comparatively rare high-pressure polymorphs discovered in heavily shocked lunar samples relative to the vast numbers of high-pressure minerals in solid Martian basalts and ordinary chondrites with high petrologic type (El Goresy et al., 2013; Tomioka & Miyahara, 2017).

5. Conclusions

As an important supplementary to the high-pressure minerals in lunar samples, we discovered reidite, a high-pressure polymorph of $ZrSiO_4$, in the KREEP-rich lunar meteorite SaU 169. The existence of reidite was confirmed by Raman spectroscopy, synchrotron XRD, and EBSD. Resembling terrestrial reidite, the lunar reidite mainly occurs as lamellae in 4 out of 40 zircons found in the regolith portion of SaU 169. Previous research shows a shock pressure of >30 GPa for reidite formation and a maximum temperature of 1473 K at ambient pressure for its preservation. It is known that impact on a porous target induces much more severe thermal metamorphism than that on a massive target. An impact on a highly porous lunar regolith with average peak pressure of ~ 10 GPa is capable of achieving a shock temperature of 1473 K. While the inferred shock pressure is lower than the typical pressure for phase transition, reidite could nevertheless have formed with the transient pressure spikes as the pressure distribution was heterogeneous in the initial stage of impact. The shock-induced high-temperature conditions in lunar regolith are not favorable for the preservation of most high-pressure minerals. It may, therefore, explain the rare findings of high-pressure minerals in regolith-derived lunar samples.

Appendix A: Estimation of the Average Peak Pressure

Internal energy increase on shock compression comprises both mechanical and thermal terms. On release of pressure, the mechanical portion (corresponding to the area under the release adiabat) is recovered (Sharp & DeCarli, 2006). Regolith breccia is composed of shock-lithified lunar regolith. Since shock experiments of Apollo regolith samples revealed that irreversible compaction of porous regolith essentially completed below 2 GPa (Ahrens & Cole, 1974) and the coefficients of thermal expansion is low, we may therefore approximate the release adiabat with the Hugoniot centered at pressure (P) and specific volume (V) of the corresponding solid with V_{os} . The residual energy (E) is approximate by

$$E \approx \frac{1}{2} (P + P_0)(V_0 - V_{os})$$

where the initial specific volume V_0 is the reciprocal of initial density and P_0 is set to be zero. Then the postshock temperature (T) can be calculated from

$$T = T_0 + \frac{E}{c_p}$$

where T_0 and c_p are the initial ambient temperature and the specific heat at constant pressure, respectively.

The properties of the lunar regolith are taken from Heiken et al. (1991), with a temperature of 280 K below 1 m, an initial density of 1.8 g/cm^3 , and a typical specific gravity of 3.1; that is, the density of the individual particles is 3.1 g/cm^3 . c_p obtained from interpolation of the experimental data (Hartlieb et al., 2016; Robie et al., 1970) is $\sim 1.1 \text{ J/gK}$. Then we can develop a positive relationship between the P and T of lunar regolith. The pressure is estimated to be ~ 10 GPa with a ~ 1473 K postshock temperature.

It must emphasize that the temperature requires seconds to achieve equilibrate with the millimeter-scale thermal inhomogeneity. The calculation was based on the assumption that the meteorite was shocked to peak pressure via a single shock and the residual energy distributed uniformly.

Conflict of Interest

The authors declare no competing financial interests.

Data Availability Statement

All data of this study can be found in the supporting information file and in a repository (<http://doi.org/10.5281/zendodo.4062618>).

Acknowledgments

We are grateful to Dr. Desmond E. Moser for helping with EBSD data interpretation. We thank the authorities from Oman for the permission to conduct this research. We thank AE Dr. Andrew J. Dombard for handling the manuscript. This manuscript has been significantly improved by the constructive reviews by Dr. Nicholas E. Timms and another anonymous reviewer. Meteorite SaU 169 was collected during the joint Omani-Swiss meteorite search in 2002. The study was financially supported by the Key Research Program of Frontier Sciences, CAS (QYZDJ-SSW-DQC001) and the Natural Science Foundation of China (41673069 and 41490631). The Omani-Swiss meteorite search campaign 2002 was supported by the Swiss National Science Foundation (2100-064929).

References

- Ahrens, T. J., & Cole, D. M. (1974). Shock compression and adiabatic release of lunar fines from Apollo 17. *Proceedings of the Fifth Lunar Conference*, Houston, TX (Supplement 5, *Geochimica et Cosmochimica Acta*), 3, 2333–2345.
- Artemieva, N., & Ivanov, B. (2004). Launch of Martian meteorites in oblique impacts. *Icarus*, 171(1), 84–101. <https://doi.org/10.1016/j.icarus.2004.05.003>
- Baer, M., & Trott, W. (2002). Mesoscale descriptions of shock-loaded heterogeneous porous materials. *AIP Conference Proceedings*, 620, 713–716. <https://doi.org/10.1063/1.1483637>
- Barrat, J.-A., Chaussidon, M., Bohn, M., Gillet, P., Göpel, C., & Lesourd, M. (2005). Lithium behavior during cooling of a dry basalt: An ion-microprobe study of the lunar meteorite Northwest Africa 479 (NWA 479). *Geochimica et Cosmochimica Acta*, 69(23), 5597–5609. <https://doi.org/10.1016/j.gca.2005.06.032>
- Bischoff, A., & Stoeffler, D. (1992). Shock metamorphism as a fundamental process in the evolution of planetary bodies: Information from meteorites. *European Journal of Mineralogy*, 4(4), 707–756. <https://doi.org/10.1127/ejm/4/4/0707>
- Bland, P. A., Collins, G. S., Davison, T. M., Abreu, N. M., Ciesla, F. J., Muxworthy, A. R., & Moore, J. (2014). Pressure–temperature evolution of primordial solar system solids during impact-induced compaction. *Nature Communications*, 5, 5451. <https://doi.org/10.1038/ncomms6451>
- Cavosie, A. J., Erickson, T. M., & Timms, N. E. (2015). Nanoscale records of ancient shock deformation: Reidite ($ZrSiO_4$) in sandstone at the Ordovician Rock Elm impact crater. *Geology*, 43(4), 315–318. <https://doi.org/10.1130/G36489.1>
- Cavosie, A. J., Timms, N. E., Ferrière, L., & Rochette, P. (2018). FRIGN zircon—The only terrestrial mineral diagnostic of high-pressure and high-temperature shock deformation. *Geology*, 46(10), 891–894. <https://doi.org/10.1130/g45079.1>
- Chen, M., Yin, F., Li, X., Xie, X., Xiao, W., & Tan, D. (2013). Natural occurrence of reidite in the Xiuyan crater of China. *Meteoritics & Planetary Science*, 48(5), 796–805. <https://doi.org/10.1111/maps.12106>
- Corfu, F., Hanchar, J. M., Hoskin, P. W., & Kinny, P. (2003). Atlas of zircon textures. *Reviews in Mineralogy and Geochemistry*, 53(1), 469–500. <https://doi.org/10.2113/0530469>
- Crow, C. A., McKeegan, K. D., & Moser, D. E. (2017). Coordinated U-Pb geochronology, trace element, Ti-in-zircon thermometry and microstructural analysis of Apollo zircons. *Geochimica et Cosmochimica Acta*, 202, 264–284. <https://doi.org/10.1016/j.gca.2016.12.019>
- Dachille, F., Zeto, R. J., & Roy, R. (1963). Coesite and stishovite: Stepwise reversal transformations. *Science*, 140(3570), 991–993. <https://doi.org/10.1126/science.140.3570.991>
- Davison, T. M., Collins, G. S., & Bland, P. A. (2016). Mesoscale modeling of impact compaction of primitive solar system solids. *The Astrophysical Journal*, 821(1), 68. <https://doi.org/10.3847/0004-637X/821/1/68>
- El Goresy, A., Gillet, P., Miyahara, M., Ohtani, E., Ozawa, S., Beck, P., & Montagnac, G. (2013). Shock-induced deformation of Shergottites: Shock-pressure and perturbations of magmatic ages on Mars. *Geochimica et Cosmochimica Acta*, 101, 233–262. <https://doi.org/10.1016/j.gca.2012.10.002>
- Erickson, T. M., Pearce, M. A., Reddy, S. M., Timms, N. E., Cavosie, A. J., Bourdet, J., et al. (2017). Microstructural constraints on the mechanisms of the transformation to reidite in naturally shocked zircon. *Contributions to Mineralogy and Petrology*, 172(1), 6. <https://doi.org/10.1007/s00410-016-1322-0>
- French, B. M. (1998). *Traces of catastrophe: A handbook of shock-metamorphic effects in terrestrial meteorite impact structures*. Houston, TX: Lunar and Planetary Institute.
- Gibbons, R., Morris, R., Horz, F., & Thompson, T. (1975). Petrographic and ferromagnetic resonance studies of experimentally shocked regolith analogs. Paper presented at 6th Lunar and Planetary Science Conference, Houston, TX.
- Glass, B. P., & Liu, S. (2001). Discovery of high-pressure $ZrSiO_4$ polymorph in naturally occurring shock-metamorphosed zircons. *Geology*, 29(4), 371–373. [https://doi.org/10.1130/0091-7613\(2001\)029<0371:DOHPZP>2.0.CO;2](https://doi.org/10.1130/0091-7613(2001)029<0371:DOHPZP>2.0.CO;2)
- Gnos, E., Hofmann, B. A., Al-Kathiri, A., Lorenzetti, S., Eugster, O., Whitehouse, M. J., et al. (2004). Pinpointing the source of a lunar meteorite: Implications for the evolution of the Moon. *Science*, 305(5684), 657–659. <https://doi.org/10.1126/science.1099397>
- Grange, M. L., Pidgeon, R. T., Nemchin, A. A., Timms, N. E., & Meyer, C. (2013). Interpreting U-Pb data from primary and secondary features in lunar zircon. *Geochimica et Cosmochimica Acta*, 101, 112–132. <https://doi.org/10.1016/j.gca.2012.10.013>
- Gucsiik, A., Zhang, M., Koeberl, C., Salje, E. K. H., Redfern, S. A. T., & Pruneda, J. M. (2004). Infrared and Raman spectra of $ZrSiO_4$ experimentally shocked at high pressures. *Mineralogical Magazine*, 68(5), 801–811. <https://doi.org/10.1180/0026461046850220>
- Güldemeister, N., Wünnemann, K., Durr, N., & Hiermaier, S. (2013). Propagation of impact-induced shock waves in porous sandstone using mesoscale modeling. *Meteoritics & Planetary Science*, 48(1), 115–133. <https://doi.org/10.1111/j.1945-5100.2012.01430.x>
- Hammersley, A., Svensson, S., Hanfland, M., Fitch, A., & Hausermann, D. (1996). Two-dimensional detector software: From real detector to idealised image or two-theta scan. *International Journal of High Pressure Research*, 14(4–6), 235–248. <https://doi.org/10.1080/08957959608201408>
- Hartlieb, P., Toifl, M., Kuchar, F., Meisels, R., & Antretter, T. (2016). Thermo-physical properties of selected hard rocks and their relation to microwave-assisted comminution. *Minerals Engineering*, 91, 34–41. <https://doi.org/10.1016/j.mineg.2015.11.008>
- Heiken, G. H., Vaniman, D. T., & French, B. M. (1991). *Lunar sourcebook—A user's guide to the Moon*. Cambridge, England: Cambridge University Press.
- Hiesinger, H., & Head, J. W. III (2006). New views of lunar geoscience: An introduction and overview. *Reviews in Mineralogy and Geochemistry*, 60(1), 1–81. <https://doi.org/10.2138/rmg.2006.60.1>
- Hu, J., & Sharp, T. G. (2017). Back-transformation of high-pressure minerals in shocked chondrites: Low-pressure mineral evidence for strong shock. *Geochimica et Cosmochimica Acta*, 215, 277–294. <https://doi.org/10.1016/j.gca.2017.07.018>
- Ito, E., & Navrotsky, A. (1985). $MgSiO_3$ ilmenite: Calorimetry, phase equilibria, and decomposition at atmospheric pressure. *American Mineralogist*, 70(9–10), 1020–1026.
- Ivanov, B. A. (2001). Mars/Moon cratering rate ratio estimates. *Space Science Reviews*, 96(1/4), 87–104. <https://doi.org/10.1023/A:1011941121102>

- Kieffer, S. W. (1971). Shock metamorphism of the Coconino sandstone at Meteor Crater, Arizona. *Journal of Geophysical Research*, 76(23), 5449–5473. <https://doi.org/10.1029/JB076i023p05449>
- Kieffer, S. W., Phakey, P. P., & Christie, J. M. (1976). Shock processes in porous quartzite: Transmission electron microscope observations and theory. *Contributions to Mineralogy and Petrology*, 59(1), 41–93. <https://doi.org/10.1007/BF00375110>
- Knittle, E., & Williams, Q. (1993). High-pressure Raman spectroscopy of ZrSiO₄: Observation of the zircon to scheelite transition at 300 K. *American Mineralogist*, 78(3–4), 245–252.
- Kowitz, A., Gündemeister, N., Reimold, W. U., Schmitt, R. T., & Wünnemann, K. (2013). Diaplectic quartz glass and SiO₂ melt experimentally generated at only 5 GPa shock pressure in porous sandstone: Laboratory observations and meso-scale numerical modeling. *Earth and Planetary Science Letters*, 384, 17–26. <https://doi.org/10.1016/j.epsl.2013.09.021>
- Kusaba, K., Syono, Y., Kikuchi, M., & Fukuoka, K. (1985). Shock behavior of zircon: Phase transition to scheelite structure and decomposition. *Earth and Planetary Science Letters*, 72(4), 433–439. [https://doi.org/10.1016/0012-821X\(85\)90064-0](https://doi.org/10.1016/0012-821X(85)90064-0)
- Langenhorst, F., & Deutsch, A. (2012). Shock metamorphism of minerals. *Elements*, 8(1), 31–36. <https://doi.org/10.2113/gselements.8.1.31>
- Leroux, H., Reimold, W. U., Koeberl, C., Hornemann, U., & Doukhan, J. C. (1999). Experimental shock deformation in zircon: A transmission electron microscopic study. *Earth and Planetary Science Letters*, 169(3–4), 291–301. [https://doi.org/10.1016/S0012-821X\(99\)00082-5](https://doi.org/10.1016/S0012-821X(99)00082-5)
- Lin, Y., Shen, W., Liu, Y., Xu, L., Hofmann, B. A., Mao, Q., et al. (2012). Very high-K KREEP-rich clasts in the impact melt breccia of the lunar meteorite SaU 169: New constraints on the last residue of the Lunar Magma Ocean. *Geochimica et Cosmochimica Acta*, 85, 19–40. <https://doi.org/10.1016/j.gca.2012.02.011>
- Liu, D., Jolliff, B. L., Zeigler, R. A., Korotev, R. L., Wan, Y., Xie, H., et al. (2012). Comparative zircon U–Pb geochronology of impact melt breccias from Apollo 12 and lunar meteorite SaU 169, and implications for the age of the imbrrium impact. *Earth and Planetary Science Letters*, 319–320, 277–286. <https://doi.org/10.1016/j.epsl.2011.12.014>
- Liu, L. (1979). High-pressure phase transformations in baddeleyite and zircon, with geophysical implications. *Earth and Planetary Science Letters*, 44(3), 390–396. [https://doi.org/10.1016/0012-821X\(79\)90078-5](https://doi.org/10.1016/0012-821X(79)90078-5)
- Lucey, P., Korotev, R. L., Gillis, J. J., Taylor, L. A., Lawrence, D., Campbell, B. A., et al. (2006). Understanding the lunar surface and space-Moon interactions. *Reviews in Mineralogy and Geochemistry*, 60(1), 83–219. <https://doi.org/10.2138/rmg.2006.60.2>
- Miyahara, M., Kaneko, S., Ohtani, E., Sakai, T., Nagase, T., Kayama, M., et al. (2013). Discovery of seifertite in a shocked lunar meteorite. *Nature Communications*, 4, 1737. <https://doi.org/10.1038/ncomms2733>
- Nemchin, A., Timms, N., Pidgeon, R., Geisler, T., Reddy, S., & Meyer, C. (2009). Timing of crystallization of the lunar magma ocean constrained by the oldest zircon. *Nature Geoscience*, 2(2), 133–136. <https://doi.org/10.1038/ngeo417>
- Nishiizumi, K., & Caffee, M. (2010). Ejection (launch) depths of lunar meteorites. Paper presented at 73rd Annual Meeting of the Meteoritical Society, New York, NY.
- Ohtani, E., Ozawa, S., Miyahara, M., Ito, Y., Mikouchi, T., Kimura, M., et al. (2011). Coesite and stishovite in a shocked lunar meteorite, Asuka-881757, and impact events in lunar surface. *Proceedings of the National Academy of Sciences*, 108(2), 463–466. <https://doi.org/10.1073/pnas.1009338108>
- Pidgeon, R. T., Nemchin, A. A., & Kamo, S. L. (2011). Comparison of structures in zircons from lunar and terrestrial impactites. *Canadian Journal of Earth Sciences*, 48(2), 107–116. <https://doi.org/10.1139/E10-037>
- Pidgeon, R. T., Nemchin, A. A., van Bronswijk, W., Geisler, T., Meyer, C., Compston, W., & Williams, I. S. (2007). Complex history of a zircon aggregate from lunar breccia 73235. *Geochimica et Cosmochimica Acta*, 71(5), 1370–1381. <https://doi.org/10.1016/j.gca.2006.11.021>
- Robie, R. A., Hemingway, B. S., & Wilson, W. H. (1970). Specific heats of lunar surface materials from 90 to 350 degrees Kelvin. *Science*, 167(3918), 749–750. <https://doi.org/10.1126/science.167.3918.749>
- Schaal, R., & Horz, F. (1980). Experimental shock metamorphism of lunar soil. Paper presented at 11th Lunar and Planetary Science Conference, Houston, TX.
- Sharp, T. G., & DeCarli, P. S. (2006). Shock effects in meteorites. In D. S. Lauretta, & H. Y. McSween, Jr. (Eds.), *Meteorites and the early solar system II* (pp. 653–677). Tucson, AZ: University of Arizona Press.
- Stöffler, D., Ryder, G., Ivanov, B. A., Artemieva, N. A., Cintala, M. J., & Grieve, R. A. F. (2006). Cratering history and lunar chronology. *Reviews in Mineralogy and Geochemistry*, 60(1), 519–596. <https://doi.org/10.2138/rmg.2006.60.05>
- Timms, N. E., Erickson, T. M., Pearce, M. A., Cavosie, A. J., Schmieder, M., Tohver, E., et al. (2017). A pressure-temperature phase diagram for zircon at extreme conditions. *Earth-Science Reviews*, 165, 185–202. <https://doi.org/10.1016/j.earscirev.2016.12.008>
- Timms, N. E., Reddy, S. M., Healy, D., Nemchin, A. A., Grange, M. L., Pidgeon, R. T., & Hart, R. (2012). Resolution of impact-related microstructures in lunar zircon: A shock-deformation mechanism map. *Meteoritics & Planetary Science*, 47(1), 120–141. <https://doi.org/10.1111/j.1945-5100.2011.01316.x>
- Tomioka, N., & Miyahara, M. (2017). High-pressure minerals in shocked meteorites. *Meteoritics & Planetary Science*, 52(9), 2017–2039. <https://doi.org/10.1111/maps.12902>
- Walton, E. L., Timms, N. E., Hauck, T. E., MacLagan, E. A., & Herd, C. D. K. (2019). Evidence of impact melting and post-impact decomposition of sedimentary target rocks from the Steen River impact structure, Alberta, Canada. *Earth and Planetary Science Letters*, 515, 173–186. <https://doi.org/10.1016/j.epsl.2019.03.015>
- Warren, P. H. (1994). Lunar and Martian meteorite delivery services. *Icarus*, 111(2), 338–363. <https://doi.org/10.1006/icar.1994.1149>
- Wieczorek, M. A., Jolliff, B. L., Khan, A., Pritchard, M. E., Weiss, B. P., Williams, J. G., et al. (2006). The constitution and structure of the lunar interior. *Reviews in Mineralogy and Geochemistry*, 60(1), 221–364. <https://doi.org/10.2138/rmg.2006.60.03>
- Wittmann, A., Kenkmann, T., Schmitt, R. T., & Stöffler, D. (2006). Shock-metamorphosed zircon in terrestrial impact craters. *Meteoritics & Planetary Science*, 41(3), 433–454. <https://doi.org/10.1111/j.1945-5100.2006.tb00472.x>
- Xie, Z., Sharp, T. G., & DeCarli, P. S. (2006). High-pressure phases in a shock-induced melt vein of the Tenham L6 chondrite: Constraints on shock pressure and duration. *Geochimica et Cosmochimica Acta*, 70(2), 504–515. <https://doi.org/10.1016/j.gca.2005.09.003>
- Zhang, A. C., Hsu, W. B., Floss, C., Li, X. H., Li, Q. L., Liu, Y., & Taylor, L. A. (2010). Petrogenesis of lunar meteorite Northwest Africa 2977: Constraints from in situ microprobe results. *Meteoritics & Planetary Science*, 45(12), 1929–1947. <https://doi.org/10.1111/j.1945-5100.2010.01131.x>